

SUPG Finite Element Simulations of Compressible Flows

Benjamin S. Kirk

benjamin.kirk@nasa.gov

NASA Lyndon B. Johnson Space Center

November 9, 2006



The physical phenomenon of interest is high-speed gas dynamics

Physics

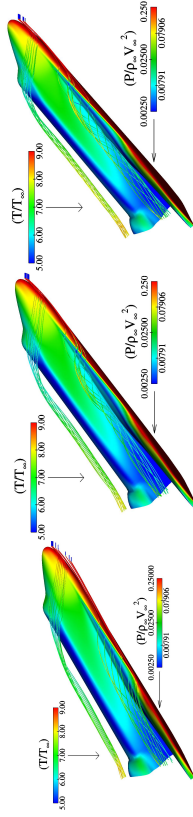
- The compressible Navier-Stokes equations describe fluid flow for *all* Mach numbers
- For aerospace applications of interest the Reynolds number is almost always such that the flows are *convection dominated*
- Transonic & greater Mach number flows usually exhibit *shockwaves*, which allow for nearly-discontinuous changes in flowfield properties

Numerics

- Discretization of the *conservation law form* of the Navier-Stokes equations is required for convergence to physically valid solutions
- Convective terms must be treated with some form of *upwinding*
- Shocks are treated with some form of *limiting* or *shock capturing*, both of which amount to artificial diffusion

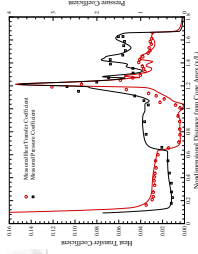
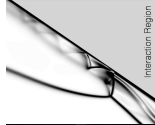


Aerodynamics



...is concerned predicting aerodynamic forces on a vehicle which result predominantly from the surface pressure distribution but also from viscous shear stress.

Aerothermodynamics



...is concerned with predicting the instantaneous heat transfer and integrated heat load into a vehicle.

The conservation of mass, momentum, and energy for a compressible fluid may be written as

$$\frac{\partial \rho}{\partial t} + \nabla \cdot (\rho \mathbf{u}) = 0 \quad (1)$$

$$\frac{\partial \rho u}{\partial t} + \nabla \cdot (\rho u u) = -\nabla P + \nabla \cdot \tau \quad (2)$$

$$\frac{\partial \rho E}{\partial t} + \nabla \cdot (\rho E \mathbf{u}) = -\nabla \cdot \mathbf{q} - P \nabla \cdot \mathbf{u} + \nabla \cdot (\tau \mathbf{u}) \quad (3)$$

where ρ is the density, \mathbf{u} is the velocity, E is the total energy per unit mass, and P is the pressure.



The viscous stress tensor $\boldsymbol{\tau}$ and the heat flux vector \mathbf{q} are defined as

$$\boldsymbol{\tau} = \mu (\boldsymbol{\nabla} \mathbf{u} + \boldsymbol{\nabla}^T \mathbf{u}) + \lambda (\boldsymbol{\nabla} \cdot \mathbf{u}) \mathbf{I} \quad (4)$$

$$q = -k \nabla T \quad (5)$$

where μ is the dynamic viscosity, λ is the second coefficient of viscosity, k is the thermal conductivity, and T is the fluid temperature. The two coefficients of viscosity are related to the bulk viscosity κ by

$$\kappa = \frac{2}{3}\mu + \lambda \quad (6)$$

In general, the bulk viscosity is negligible except in detailed studies of shock wave structure or for investigations of the adsorption and attenuation of acoustic waves [1]. Under this assumption, $\kappa = 0$ in Equation (6) and λ is defined as

$$\lambda = -\frac{2}{3}\mu_s \quad (7)$$

Equation (4) with (7) is known as Stokes' hypothesis for a Newtonian fluid [2].



- The choice of the *conserved variables* $\mathbf{U} = [\rho, \rho u, \rho v, \rho w, \rho E]^T$ is convenient for high-speed compressible flows ($M \gtrsim 0.3$) as it allows for explicit algorithms for (9).
- Other choices are possible which have applicability to a larger range of flow problems [3]
- Equation (9) may be transformed for any set of variables \mathbf{V} via $\mathbf{U} = \mathbf{A}_0 \mathbf{V}$ where $\mathbf{A}_0 \equiv \frac{\partial \mathbf{U}}{\partial \mathbf{V}}$.
- Ease of applying boundary conditions varies widely with variable choice



Godunov's theorem [4] is particularly relevant for numerical methods applied to high-speed gas dynamics:

Any linear monotone scheme cannot be better than first-order accurate.

For the model linear convection-diffusion problem

$$-\varepsilon \Delta u + \mathbf{v} \cdot \nabla u = f$$

with \mathbf{v} specified independently of u this implies two important results

- 1 Linear second-order (or higher) accurate schemes cannot be monotone
- 2 Even for linear problems, a monotone second-order (or higher) scheme is necessarily nonlinear

which have important implications going forth on the interplay between upwinding, shock capturing, and solution limiting.



The Streamline-Upwind Petrov-Galerkin Finite Element Method



SUPG stabilization does not yield monotone solutions. Additional treatment is needed to prevent spurious oscillations in regions of shockwaves. Hence (11) is augmented with a *shock capturing* term to produce the augmented weak form: *find \mathbf{U} such that*

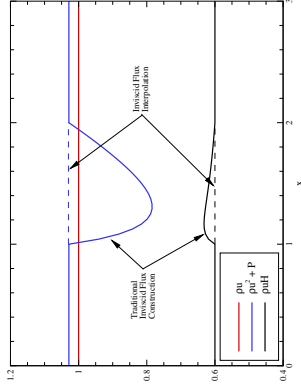
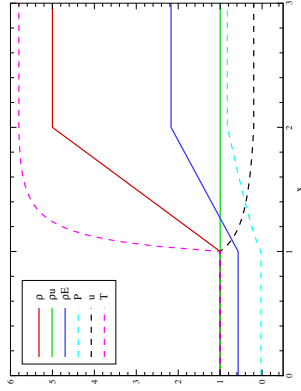
$$\begin{aligned} & \int_{\Omega} \left[\mathbf{W} \cdot \left(\frac{\partial \mathbf{U}}{\partial t} + \mathbf{A}_i \frac{\partial \mathbf{U}}{\partial x_i} \right) + \frac{\partial \mathbf{W}}{\partial x_i} \cdot \left(\mathbf{K}_{ij} \frac{\partial \mathbf{U}}{\partial x_j} \right) \right] d\Omega \\ & + \sum_{e=1}^{n_{el}} \int_{\Omega_e} \tau_{SUPG} \frac{\partial \mathbf{W}}{\partial x_k} \cdot \mathbf{A}_k \left[\frac{\partial \mathbf{U}}{\partial t} + \mathbf{A}_i \frac{\partial \mathbf{U}}{\partial x_i} - \frac{\partial}{\partial x_i} \left(\mathbf{K}_{ij} \frac{\partial \mathbf{U}}{\partial x_j} \right) \right] d\Omega \\ & + \sum_{e=1}^{n_{el}} \int_{\Omega_e} \delta \left(\frac{\partial \mathbf{W}}{\partial x_i} \cdot \frac{\partial \mathbf{U}}{\partial x_i} \right) d\Omega = \int_{\Gamma} \mathbf{W} \cdot \mathbf{g} d\Gamma \quad (12) \end{aligned}$$

for all \mathbf{W} in an appropriate function space

A definition of δ may be found in [5, 6]. Note that consistency is lost with (9) and a discretization of (12) is only first-order in regions of appreciable δ .



Inviscid Flux Discretization



The semidiscrete weak form in equation (12) is discretized in time using a backwards finite difference scheme. Both first and second-order accurate in time schemes may be derived from Taylor series expansions in time about U_{n+1} :

$$U_n = U_{n+1} + \frac{\partial U_{n+1}}{\partial t} (t_n - t_{n+1}) + \frac{\partial^2 U_{n+1}}{\partial t^2} \frac{(t_n - t_{n+1})^2}{2} + \mathcal{O}\left((t_n - t_{n+1})^3\right)$$

$$U_{n-1} = U_{n+1} + \frac{\partial U_{n+1}}{\partial t} (t_{n-1} - t_{n+1}) + \frac{\partial^2 U_{n+1}}{\partial t^2} \frac{(t_{n-1} - t_{n+1})^2}{2} + \mathcal{O}\left((t_{n-1} - t_{n+1})^3\right)$$

which, upon substituting $t_{n+1} - t_n \equiv \Delta t_{n+1}$ and $t_{n+1} - t_{n-1} = \Delta t_{n+1} + \Delta t_n$, becomes

$$U_n = U_{n+1} - \frac{\partial U_{n+1}}{\partial t} \Delta t_{n+1} + \frac{\partial^2 U_{n+1}}{\partial t^2} \frac{\Delta t_{n+1}^2}{2} - \mathcal{O}\left(\Delta t_{n+1}^3\right)$$

$$U_{n-1} = U_{n+1} - \frac{\partial U_{n+1}}{\partial t} (\Delta t_{n+1} + \Delta t_n) + \frac{\partial^2 U_{n+1}}{\partial t^2} \frac{(\Delta t_{n+1} + \Delta t_n)^2}{2} - \mathcal{O}\left((\Delta t_{n+1} + \Delta t_n)^3\right)$$

The semidiscrete weak form in equation (12) is discretized in time using a backwards finite difference scheme. Both first and second-order accurate in time schemes may be derived from Taylor series expansions in time about U_{n+1} :

$$U_n = U_{n+1} + \frac{\partial U_{n+1}}{\partial t} (t_n - t_{n+1}) + \frac{\partial^2 U_{n+1}}{\partial t^2} \frac{(t_n - t_{n+1})^2}{2} + \mathcal{O}\left((t_n - t_{n+1})^3\right)$$

$$U_{n-1} = U_{n+1} + \frac{\partial U_{n+1}}{\partial t} (t_{n-1} - t_{n+1}) + \frac{\partial^2 U_{n+1}}{\partial t^2} \frac{(t_{n-1} - t_{n+1})^2}{2} + \mathcal{O}\left((t_{n-1} - t_{n+1})^3\right)$$

which, upon substituting $t_{n+1} - t_n \equiv \Delta t_{n+1}$ and $t_{n+1} - t_{n-1} = \Delta t_{n+1} + \Delta t_n$, becomes

$$U_n = U_{n+1} - \frac{\partial U_{n+1}}{\partial t} \Delta t_{n+1} + \frac{\partial^2 U_{n+1}}{\partial t^2} \frac{\Delta t_{n+1}^2}{2} - \mathcal{O}\left(\Delta t_{n+1}^3\right)$$

$$U_{n-1} = U_{n+1} - \frac{\partial U_{n+1}}{\partial t} (\Delta t_{n+1} + \Delta t_n) + \frac{\partial^2 U_{n+1}}{\partial t^2} \frac{(\Delta t_{n+1} + \Delta t_n)^2}{2} - \mathcal{O}\left((\Delta t_{n+1} + \Delta t_n)^3\right)$$

Which can be rewritten for $\frac{\partial U_{n+1}}{\partial t}$ as:

$$\frac{\partial \mathbf{U}_{n+1}}{\partial t} = \frac{\mathbf{U}_{n+1}}{\Delta t_{n+1}} - \frac{\mathbf{U}_n}{\Delta t_{n+1}} + \frac{\partial^2 \mathbf{U}_{n+1}}{\partial t_{n+1}^2} - \frac{\mathcal{O}(\Delta t_{n+1}^2)}{2} \quad (18)$$

$$\begin{aligned}
\frac{\partial \mathbf{U}_{n+1}}{\partial t} = & \frac{\mathbf{U}_{n+1}}{\Delta t_{n+1} + \Delta t_n} - \frac{\mathbf{U}_{n-1}}{\Delta t_{n+1} + \Delta t_n} + \frac{\partial^2 \mathbf{U}_{n+1} (\Delta t_{n+1} + \Delta t_n)}{\partial t^2} \\
& - \mathcal{O} \left((\Delta t_{n+1} + \Delta t_n)^2 \right)
\end{aligned}
\tag{19}$$



The familiar backwards Euler time discretization follows directly from (18) by recognizing

$$\frac{\partial \mathbf{U}_{n+1}}{\partial t} = \frac{\mathbf{U}_{n+1} - \mathbf{U}_n}{\Delta t_{n+1}} + \mathcal{O}(\Delta t_{n+1}) \quad (20)$$

which provides a first-order in time approximation upon neglecting the $\mathcal{O}(\Delta t_{n+1})$ term.



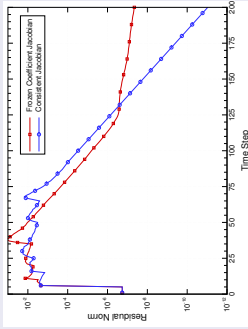
A linear combination of $\left(1 + \frac{\Delta t_{n+1}}{\Delta t_n}\right) \times (18)$ and $-\frac{\Delta t_{n+1}}{\Delta t_n} \times (19)$ can be used to annihilate the leading $\frac{\partial^2 U_{n+1}}{\partial t^2}$ term to create a backwards, second-order accurate approximation to $\frac{\partial U_{n+1}}{\partial t}$. This approximation, along with (20), can be generalized in the form

$$\frac{\partial U_{n+1}}{\partial t} = \alpha_t U_{n+1} + \beta_t U_n + \gamma_t U_{n-1} + \mathcal{O}\left(\Delta t_{n+1}^p\right) \quad (21)$$

to yield either a first or second-order accurate scheme. The weights α_t , β_t , and γ_t are given below for $p = 1$ and $p = 2$.

p	α_t	β_t	γ_t
1	$\frac{1}{\Delta t_{n+1}}$	$\frac{-1}{\Delta t_{n+1}}$	0
2	$-\beta_t - \gamma_t$	$-\left[\frac{1}{\Delta t_{n+1}} + \frac{1}{\Delta t_n}\right]$	$\frac{\Delta t_{n+1}}{\Delta t_n(\Delta t_{n+1} + \Delta t_n)}$

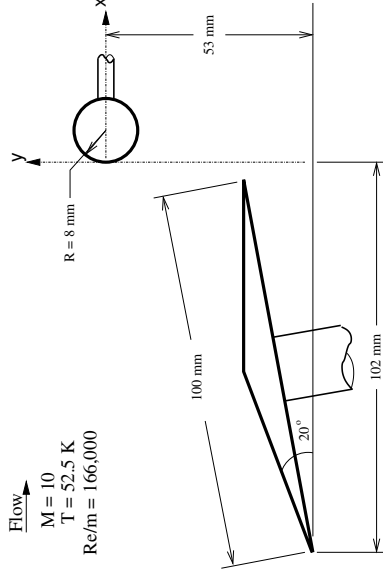
- Time-marching to steady-state is almost always used for high-speed flows
- Implicit techniques required for viscous problems with tight wall spacing
- For steady problems, at each time step the resulting nonlinear problem is usually solved only approximately (usually 1 Newton step)
- DOF coupling defined via standard finite element basis function overlap
- Matrix-free GMRES with block-diagonal preconditioning used in earlier work [6]
- I have used matrix & matrix-free GMRES with full ILU-0 preconditioning – *linearization is important*



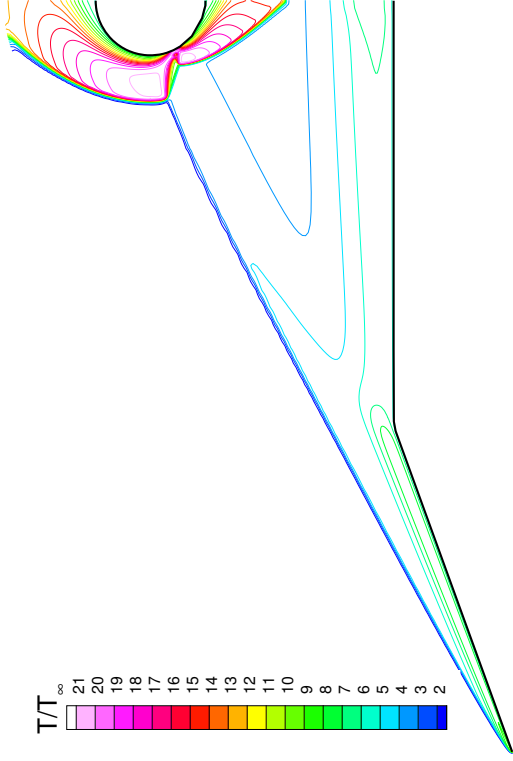
Influence of linearization strategy on iterative convergence for Mach 3 flow over a cylinder



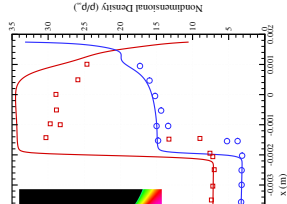
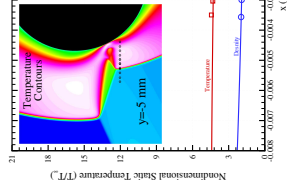
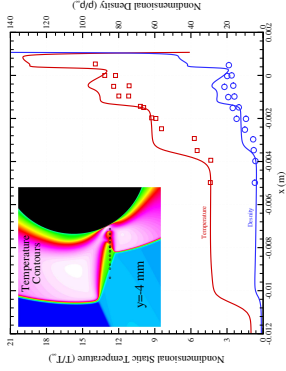
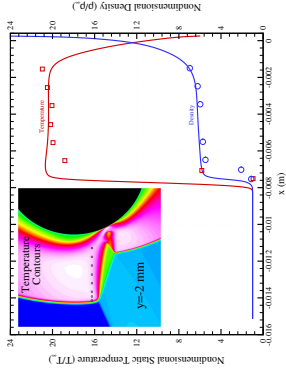
An experimental test program was conducted in 1998 by France's Office National d'Etudes et de Recherches Aéropatiales (ONERA) to investigate shock-shock interactions produced by an oblique shock impinging on the bow shock of a cylinder [8]. This configuration is examined here to assess the quality of surface heat transfer predictions.



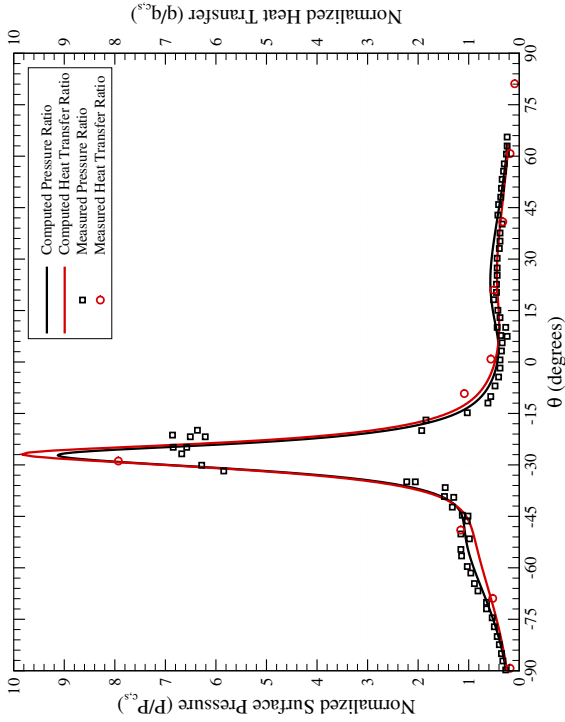
Static temperature contours



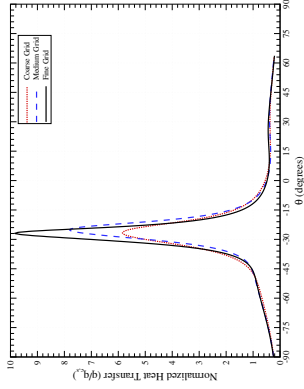
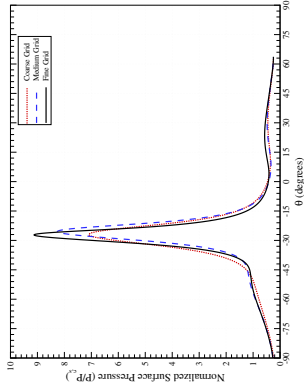
Type IV Shock Interaction



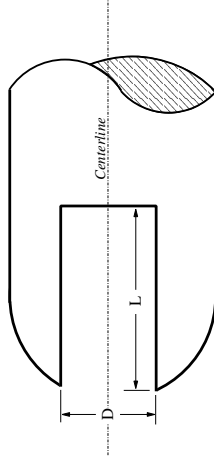
Type IV Shock Interaction



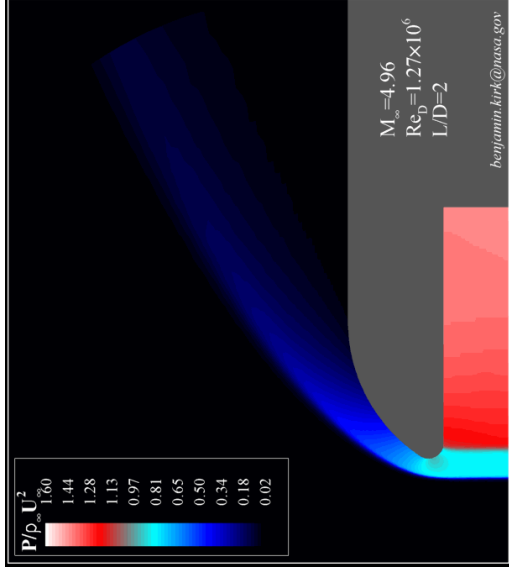
Type IV Shock Interaction



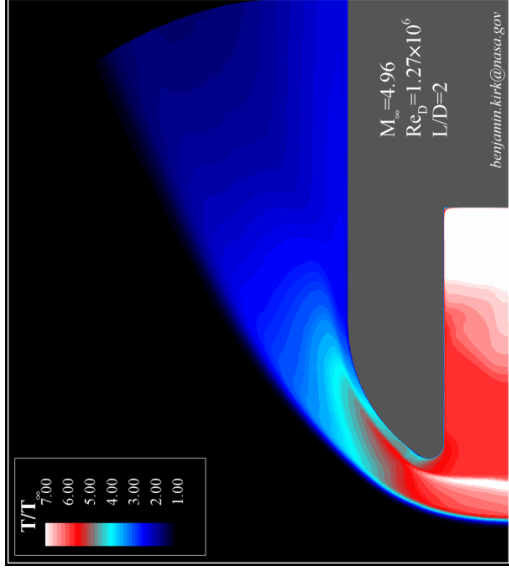
Hypersonic flow over a missile nose tip with a forward facing cavity is considered. This configuration, shown schematically below, has been observed to exhibit transient flowfield response in both experimental investigations and numerical simulations. [9, 10] The flowfield response characteristics are largely driven by the cavity length-to-diameter ratio (L/D). Experimental studies in conventional tunnels report oscillatory response even for relatively shallow cavities, suggesting a threshold L/D of 0.4. Numerical simulations predict a higher threshold L/D of approximately 1.25 for transient response. Subsequent studies in a quiet wind tunnel verify the computational results, indicating freestream noise is the mechanism for driving unsteady response in shallow cavities. [11]



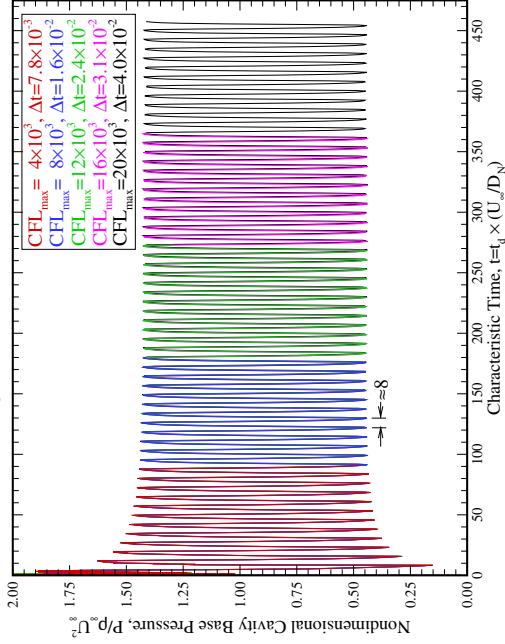
Forward-Facing Cavity



Forward-Facing Cavity



The Figure below shows the cavity base pressure vs. time for the series of simulations which were conducted to assess time convergence.



Observations

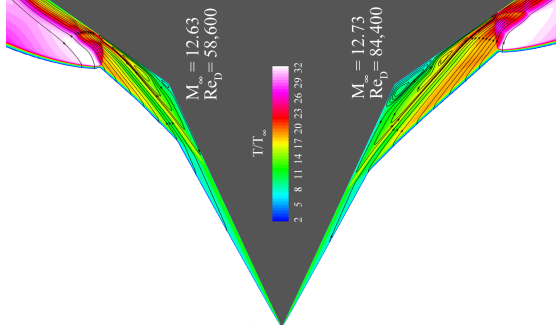
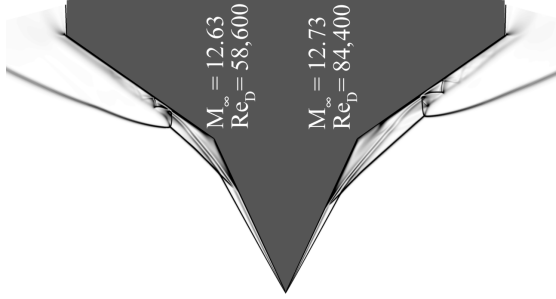
- Four Reynolds numbers were tested in the nominally Mach 14 nozzle
- No appreciable vibrational nonequilibrium effects observed
- Highly unsteady flow observed for *all* Reynolds numbers tested
- For a uniform freestream, CFD predicts steady flow for the two lowest Reynolds numbers

Run	2890	2891	2893	2894
M_∞	13.6	13.17	12.73	12.63
Re_D	1.12×10^6	4.11×10^5	8.44×10^4	5.86×10^4
ρ_∞	7.8077×10^{-3}	2.9604×10^{-3}	5.8967×10^{-4}	3.9783×10^{-4}
U_∞	2006.6	1949.8	1763.5	1682.6
T_∞	52.3	52.7	46.1	42.7
				kg/m^3 m/sec K



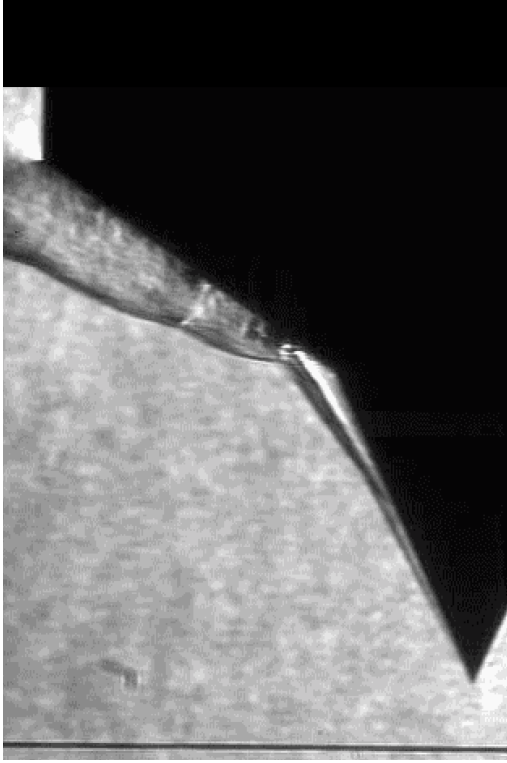
AEDC Sharp Double Cone

Steady states, runs 2893 and 2894



AEDC Sharp Double Cone

High speed schlieren, run 2890



AEDC Sharp Double Cone

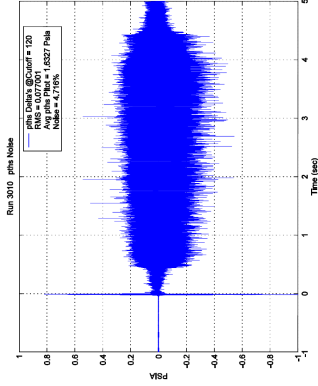
Ongoing Work

- For a uniform inflow, CFD converges to a steady-state for the two lowest Reynolds numbers tested
- This is in contrast to the experimental results
- My conjecture is that freestream noise drives the unsteady behavior at these low Reynolds number
- Current analysis is focused on testing this theory



AEDC Sharp Double Cone

Noise Characterization [14]



AEDC Sharp Double Cone

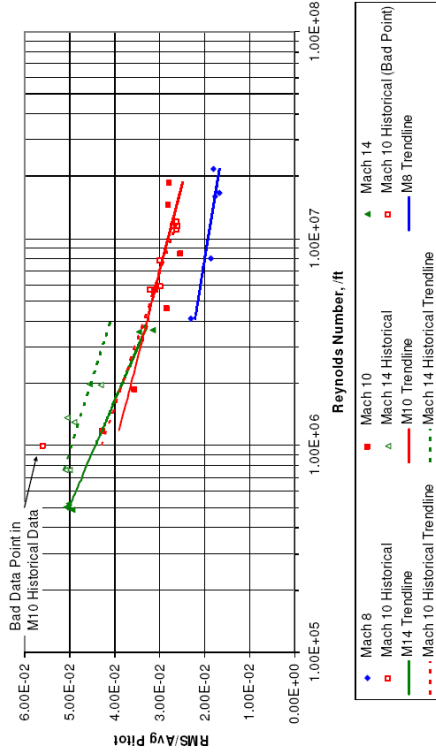
Noise Characterization [14]

$$y = -0.0032\ln(x) + 0.0709 \quad M8$$

$$y = -0.0051\ln(x) + 0.1102 \quad M10$$

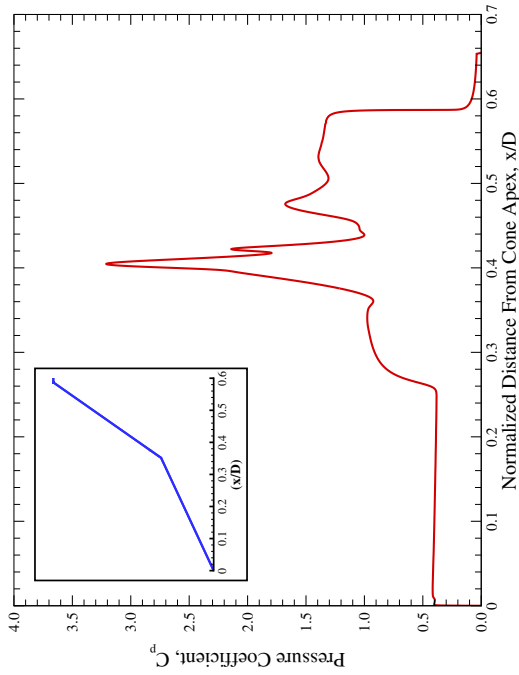
$$y = -0.0086\ln(x) + 0.1628 \quad M14$$

Variation of Pitot Pressure Fluctuation With Varying Reynolds Number



AEDC Sharp Double Cone

Preliminary Results – Surface Pressure





J. C. Tannehill, D. A. Anderson, and R. H. Pletcher.
Computational Fluid Mechanics and Heat Transfer.
Taylor & Francis, Washington, D.C., 2nd edition, 1997.



Ronald L. Panton.
Incompressible Flow.
John Wiley & Sons, 2nd edition, 1996.



G. Hauke and T. J. R. Hughes.
A comparative study of different sets of variables for solving compressible and incompressible flows.
Computer Methods in Applied Mechanics and Engineering, 153:1–44, 1998.



S. K. Godunov.
Finite difference methods for numerical computation of discontinuous solutions of the equations of fluid dynamics.
Mat. Sbornik, 47:271–295, 1959.



G. J. LeBeau.
The finite element computation of compressible flows.
Master's thesis, The University of Minnesota, 1990.



S. K. Aliabadi.
Parallel Finite Element Computations in Aerospace Applications.
PhD thesis, The University of Minnesota, 1994.



L. Catabriga and A. L. G. A. Coutinho.
Improving convergence to steady state of implicit SUPG solution of Euler equations.
Communications in Numerical Methods in Engineering, 18(5):345–353, May 2002.



T. Pot, B. Chanetz, M. Lefebvre, and P. Bouchardy.
Fundamental study of shock/shock interference in low density flow.
21st International Symposium on Rarefied Gas Dynamics, 1998.





W. A. Engblom and D. B. Goldstein.

Nose-tip surface heat reduction mechanism.

34th AIAA Aerospace Sciences Meeting and Exhibit, AIAA Paper 1996-354, January 1996.



Sidra I. Siliton and David B. Goldstein.

Ablation onset in unsteady hypersonic flow about nose tip with cavity.

Journal of Thermophysics and Heat Transfer, 14(3):421–434, July–September 2000.



W. A. Engblom, D. B. Goldstein, D. Landoon, and S. P. Schneider.

Fluid dynamics of hypersonic forward-facing cavity flow.

34th AIAA Aerospace Sciences Meeting and Exhibit, AIAA Paper 1996-667, January 1996.



Ioannis Nompelis, Graham V. Candler, and Michael S. Holden.

Effect of Vibrational Nonequilibrium on Hypersonic Double-Cone Experiments.

AIAA Journal, 41(11):2162–2169, November 2003.



Joseph J. Coblish, Michael S. Smith, Terrell Hand, Graham V. Candler, and Ioannis Nompelis.

Double-Cone Experiment and Numerical Analysis at AEDC Hypervelocity Wind Tunnel No. 9.

43rd AIAA Aerospace Sciences Meeting and Exhibit, AIAA Paper 2005-0902, January 2005.



J. McNalley.

Pitot Noise Measurement During FY06 NASA MSL Test.

Arnold Engineering Development Center Memorandum, September 2006.

